In situ imaging and spectroscopy of single-wall carbon nanotube synthesis by laser vaporization

A. A. Puretzky, D. B. Geohegan,[a] X. Fan, and S. J. Pennycook
Solid State Division, Oak Ridge National Laboratory, Oak Ridge, Tennessee 37831

(Received 9 September 1999; accepted for publication 10 November 1999)

The synthesis of single-wall carbon nanotubes by Nd:YAG laser vaporization of a graphite/(Ni, Co) target is investigated by laser-induced luminescence imaging and spectroscopy of Co atoms, C_2 and C_3 molecules, and clusters at 1000 °C in flowing 500 Torr Ar. These laser-induced emission images under typical synthesis conditions show that the plume of vaporized material is segregated and confined within a vortex ring which maintains a ~1 cm^3 volume for several seconds. Using time-resolved spectroscopy and spectroscopic imaging, the time for conversion of atomic and molecular species to clusters was measured for both carbon (200 μs) and cobalt (2 ms). This rapid conversion of carbon to nanoparticles, combined with transmission electron microscopy analysis of the collected deposits, indicate that nanotube growth occurs over several seconds in a plume of mixed nanoparticles. By adjusting the time spent by the plume within the high-temperature zone using these *in situ* diagnostics, single-walled nanotubes of controlled length were grown at an estimated rate of 0.2 μm/s. © *2000 American Institute of Physics.* [S0003-6951(00)02102-1]

The remarkable electronic and structural properties of carbon nanotubes promise to revolutionize application areas from nanoscale electronics to ultralightweight structural materials.[1] Since electronic transport in single-wall carbon nanotubes (SWNT) is directly related to their atomic structure, it is essential to understand what controls nanotube size and structure during synthesis. Furthermore, methods for large-scale production of SWNT have not been developed because so little is understood about the synthesis process.

Up until now, three principal methods have been used to synthesize carbon nanotubes. These include laser vaporization (LV),[2] dc-arc vaporization (AV),[3,4] and chemical vapor deposition (CVD).[5,6] Unlike CVD, both LV and AV now produce nearly exclusively SWNT. However, very little is known about where and when the SWNT are formed in LV or AV growth chambers, the identity of the precursor species, and the growth rates.

Pulsed LV is especially amenable to diagnostic investigations. The vaporizing pulse lasts only ~10 ns and SWNT growth then can occur undisturbed from further excitation, even for single laser ablation events.[7] Recent spectroscopic measurements of the luminous laser plasma have been made for pulsed LV at early times after Nd:YAG laser ablation (<200 μs)[8] and after long-pulse CO_2 laser ablation at room temperature.[9] However, these measurements were limited to times while the ablated material is still quite hot.

Recently, laser induced luminescence (LIL), gated intensified charge-coupled device (ICCD) imaging, and optical emission spectroscopy were applied to understand how nanoparticles form and grow in pulsed laser ablation plumes at room temperature.[10–12] In this study these techniques are applied to investigate SWNT growth under typical ablation conditions at high temperatures.

The SWNT growth setup in Fig. 1 was fashioned after that used by Guo *et al.*[2] It consists of a quartz tube (2 in. diameter, 24 in. length) mounted inside a hinged tube furnace (12 in. length) operating at 1000 °C. The quartz tube was O-ring sealed to standard 4.5-in.-Conflat vacuum components. The ablation and probe laser beams entered through the same Suprasil window which was mounted in a vacuum flange. Argon gas was introduced around this window, controlled at 100 sccm to maintain a 500 Torr pressure, and pumped out through a needle valve downstream of a brass, water-cooled collector which was inserted as shown.

A 1-in.-diameter graphite target containing 1 at. % each of Ni (Alfa, 2.2–3.0 μm, 99.9%) and Co (Alfa, 1–6 μm, 99.8%) powders was prepared with the carbon cement (Dylon GC) procedure described in Ref. 2. The target was screwed onto a 0.25-in.-diameter graphite rod and was rotated during operation. The ablation laser beam (single 8 ns pulses, 140 mJ of combined 1.06 μm and 532 nm outputs) was focused to a 1.6-mm-diameter donut-shaped spot on the target. An unfocused, time-delayed XeCl-laser (308 nm, 30 ns pulse, 20 mJ/cm^2) was used to induce luminescence in the ablation plume.

The furnace was opened for ~3 s to permit imaging of the plume with a gated ICCD-camera system (Princeton Instruments, 5-ns-minimum gate, 200–820 nm spectral range).

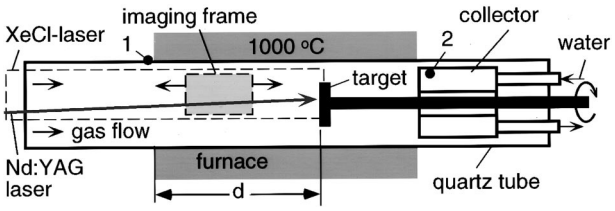

FIG. 1. Schematic of the 2-in.-diameter quartz tube and hot furnace used for laser vaporization growth of SWNT with *in situ* LIL imaging and spectroscopy diagnostics. Beam geometries and imageable area are indicated. The black dots and the numbers show the collection points of the ablated material: (1) upstream; (2) collector. The C/Ni/Co target was positioned at different distances, *d*, from the front of the furnace.

[a]Electronic mail: odg@ornl.gov

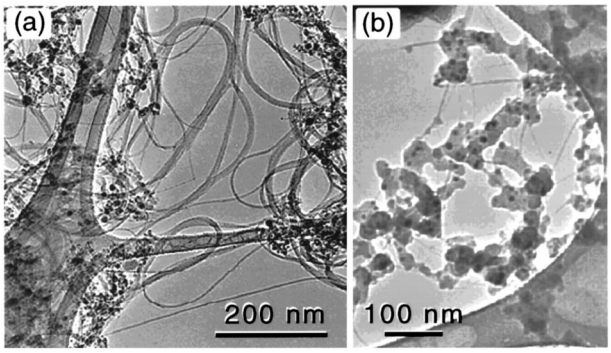

FIG. 2. TEM images of the raw soot collected: (a) downstream on the collector (point 2, for $d=21$ cm in Fig. 1), showing a very high fraction of SWNT bundles along with metal nanoparticles (black dots); (b) upstream (point 1, for $d=12.5$ cm in Fig. 1) showing short (~100 nm) SWNT in the early stages of growth, controlled by limiting the growth time to 0.5 s.

At each plume location, the plasma emission and/or laser-induced luminescence was collected for optical emission spectroscopy using a 0.3 m spectrometer (Acton VM-503, resolution either 10 or 1.3 nm) with an intensified, gated diode array (Princeton Instrument IRY-700RB).

As shown in Fig. 2(a), ~10-μm-long SWNT bundles comprised very high fractions of the deposit found downstream on the collector (>70%–90% as estimated from field-emission SEM analysis) when the target was positioned $d=21$ cm from the front of the furnace. Metal catalyst (<20 nm diameter) and small amounts of amorphous carbon nanoparticles accounted for the rest of the deposit (as described in the literature).[2] EELS investigation of individual metal-catalyst nanoparticles (using a 0.3-nm-diameter electron beam) revealed that their compositions were reproducibly $Ni_xCo_y(x\approx y\approx 0.5)$, with both Ni and Co uniformly distributed inside each nanoparticle to within sub-nm dimensions.

To determine where and when SWNT growth occurred, LIL-ICCD imaging and spectroscopy of the C/Ni/Co plume were performed at different times after laser vaporization, Δt, spanning $20\,\text{ns}\leqslant\Delta t\leqslant 3$ s. For $\Delta t\leqslant 0.2$ ms, a series of shocks within the plume[13,14] results in segregation of the ablated material into the vortex ring[15,16] (or ''smoke ring'')[10] shown at $\Delta t=0.2$ ms in Figs. 3(a) and 3(b). As shown in Fig. 3(a), the vortex motion efficiently traps aggregated nanoparticles in a confined volume for long times (~3 s within ~1 cm^3 in this study).

The leading edge of the plume propagates with velocities of: 10^3 cm/s between $200\,\mu\text{s}<\Delta t<2$ ms; 50 cm/s for $10\,\text{ms}<\Delta t<50$ ms; and 6 cm/s at $30\,\text{ms}<\Delta t<200$ ms. After $\Delta t=2$ s the plume stops moving upstream, and the plane of the vortex ring tilts toward the tube axis, possibly due to flow currents or thermophoretic forces. The plume is then dragged by the gas flow back to the collector with an estimated flow velocity of 0.6 cm/s. Finally, nanotubes, metal catalyst particles and unconverted carbon soot deposit on the cool collector surface by thermophoresis.[12] LIL-ICCD imaging ensured that all deposits and images were collected without interference from previous laser shots using laser repetition rates less than 0.016 Hz.

Optical emission spectra were obtained for each image. Figure 4 presents a short summary. At early times in the plume expansion, emission from excited states in the plasma

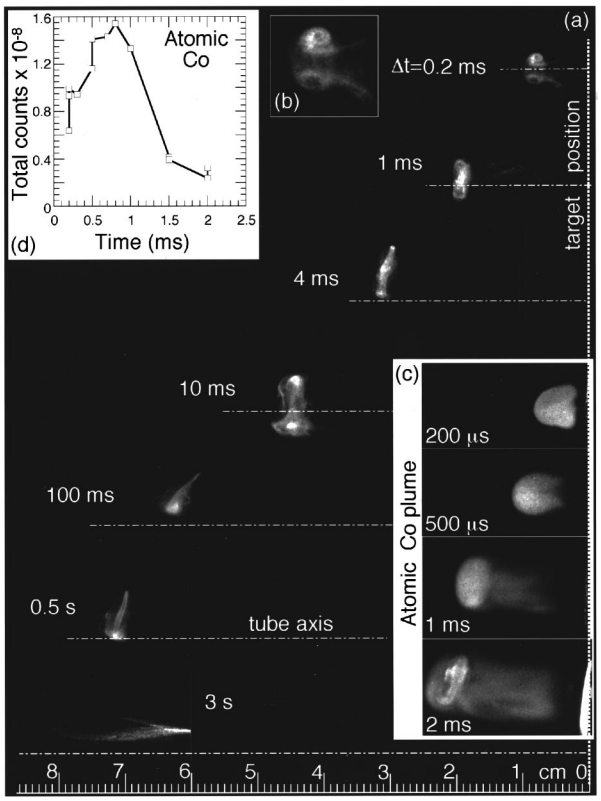

FIG. 3. Laser-induced luminescence (LIL) images of the C/Ni/Co plume during SWNT synthesis. A Nd:YAG laser vaporizes a C/Co/Ni target (right edge of figure) inside a 2-in.-quartz tube at 1000 °C in 500 Torr Ar (flowing to the right at 100 sccm, ~0.6 cm/s at the center of the tube). Each image represents a different ablation event. (a) Unfiltered images show the location of all C/Co/Ni species during nanotube growth (100 ns gate width, opened $\Delta\tau=100$ ns after the XeCl-laser pulse); (b) selective imaging in the 320–380 nm spectral region to locate ground-state atomic Co in the plume (100 ns gate width, $\Delta\tau=0$); (c) temporal history of the total number density of ground-state atomic Co, determined from integrating the LIL from a complete set of atomic-Co images shown in (b).

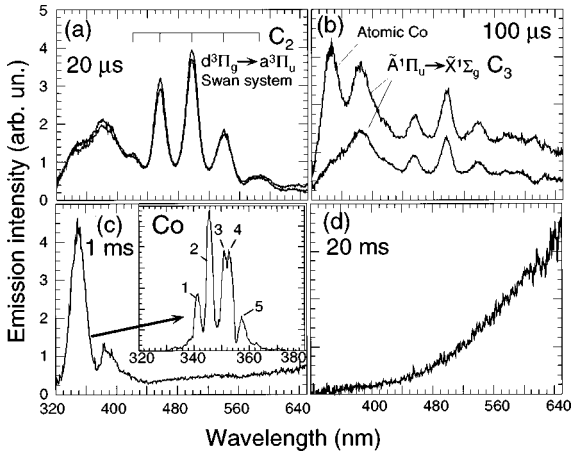

FIG. 4. Plasma emission (dashed) and laser-induced luminescence (solid) spectra measured at different time delays after the ablation laser pulse, Δt, and distances, x, from the target: (a) $\Delta t=20\,\mu$s, $x=0.2$ cm; (b) $\Delta t=100\,\mu$s, $x=0.5$ cm; (c) $\Delta t=1$ ms, $x=2$ cm; and (d) $\Delta t=20$ ms, $x=5$ cm. Acquisition times of 100 ns [(a), (b)] and 3.5 μs [(c), (d)] began 50 ns after the XeCl-laser pulse. The inset in (c) shows a 1.3-nm-resolution spectrum of induced fluorescence from the following transitions: (1) $b^4F_{7/2}-y^2G^0_{9/2}$ at 341.23 nm; (2) $b^4F_{9/2}-y^4G^0_{11/2}$ at 345.35 nm; (3) $b^4F_{5/2}-y^4G^0_{7/2}$ at 350.98 nm; (4) $b^4F_{7/2}-y^4G^0_{9/2}$ at 352.98 nm; and (5) $b^4F_{5/2}-y^4D^0_{5/2}$ at 357.50 nm.

dominates any laser-induced luminescence. As in Fig. 4(a), the $d^3\Pi_g \rightarrow a^3\Pi_u$ Swan system of C_2 and the $A^1\Pi_u \rightarrow X^1\Sigma_g$ band C_3 are prominent at these times. Later when the plasma expands, cools, and recombines, the 308-nm-XeCl laser can induce emission by pumping transitions from the ground states: of C_3 (via $A^1\Pi_u \leftarrow X^1\Sigma_g$); of atomic Co (via $a^4F_J \leftarrow y^4G^0_J$); and of atomic Ni (via $a^3D_1 \leftarrow y^3D^0_2$).

In addition, blackbody radiation can be induced from carbon clusters,[17] nanoparticles,[18] and nanotubes. The intensity of this blackbody emission, I, is defined by $I = Ar^3(T_0 + \Delta T)^5$ where T_0 is the initial temperature of the cluster, ΔT is the temperature increase due to laser-heating, A is a constant, and r is the cluster radius. This radiation becomes observable coincident with the disappearance of the C_2 and C_3 bands in both the plasma emission and the laser-induced spectra for $\Delta t > 200\ \mu$s at 1000 °C (and $\Delta t > 100\ \mu$s at room temperature). We conclude that nearly all of the carbon in the plume has converted into clusters or larger aggregates by these times.

However, the Co in the plume remains in atomic form until much later. As shown in Figs. 3(c) and 4(c), the ground-state Co population peaks at $\Delta t = 0.8$ ms and drops by an order of magnitude by $\Delta t = 2$ ms, permitting estimates of the Co clustering time of ~2 ms at 1000 °C (~1 ms at room temperature). Blackbody radiation remains the only feature of the spectra taken at all later times [Fig. 4(d)].

Further evidence of the sequential condensation of carbon and cobalt into clusters is the relatively uniform spatial distribution of atomic Co in the plume for $\Delta t < 2$ ms compared to the vorticity of the clustered carbon material [compare Figs. 3(a) and 3(b)]. We believe that the higher diffusivity of the atomic Co effectively competes with the hydrodynamic trapping during this time. Only the leading edge of the atomic-Co plume overlaps the carbon-cluster vortex ring during the condensation of the Co atoms. The Ni_xCo_y alloy particles indicate similar condensation times for Ni and Co. It is quite possible that the carbon clusters serve as condensation centers for metal cluster growth.

Both imaging and spectroscopy indicate that within the first few milliseconds after laser ablation, atoms and molecules of both carbon and metal catalyst disappear due to condensation into nanoparticles. Unless SWNTs grow very rapidly from atoms and molecules within these first few milliseconds, the majority of growth appears to occur from a feedstock of mixed nanoparticles over seconds of annealing time.

In order to check this conclusion and estimate the SWNT growth rate, the target was positioned at several distances from the front furnace edge to adjust the time spent within the hot zone before exiting the furnace in the upstream direction. LIL-ICCD imaging recorded the plume dynamics from ablation to deposition and the collected deposits were examined by TEM.

Figure 2(b) shows a TEM image of a deposit collected for a target position of $d = 12.5$ cm (see Fig. 1), where LIL-ICCD imaging measured a time of 0.5–0.7 s spent by the plume inside the furnace. The collected material consists of aggregated carbon and metal-catalyst nanoparticles, and thin SWNT bundles of only ~100 nm length, yielding an average growth rate of 0.2 μm/s at 1000 °C. The relative yield of the carbon particles is much larger than the yield of the carbon nanotubes which clearly shows that the time spent by the plume in the hot zone (~0.5 s) was not sufficient to convert all of the carbon material into nanotubes.

In summary, these results confirm the conclusions of the time-resolved imaging and spectroscopy measurements (along with *ex situ* TEM, EELS, and FESEM). Although SWNT may initiate growth during the first few milliseconds after laser ablation, the majority of growth occurs inside the oven from a mixture of gas-suspended carbon and metal-catalyst nanoparticles which are hydrodynamically trapped in a vortex ring within a ~1 cm^3 volume for several seconds. The spectroscopy at early times after laser ablation indicates that the plume initially consists of atomic and molecular species, with no evidence of hot molten particulates which were recently suggested as the primary ejecta.[19] Condensation of carbon occurs within 0.2 ms after ablation, while atomic Co condenses much later (between 1.5 and 2 ms). Through these images of the growth process, we conclude that long (~10 μm) SWNT can form from the small amount of material vaporized in a single-laser shot, a remarkable feat of self-assembly.

The authors gratefully acknowledge research assistance by M. L. Simpson, M. Guillorn, and helpful conversations with D. J. Rader. This work was sponsored by the Division of Material Science, U.S. Department of Energy under Contract No. DE-AC05-96-R22464 with Lockheed Martin Energy Research Corp.

[1] B. Yakobson and R. E. Smalley, Am. Sci. **85**, 324 (1997).
[2] T. Guo, P. Nikolaev, A. Thess, D. T. Colbert, and R. E. Smalley, Chem. Phys. Lett. **236**, 419 (1995).
[3] T. S. Iijima and T. Ichihashi, Nature (London) **363**, 603 (1993).
[4] C. Journet, W. K. Maser, P. Bernier, A. Loiseau, M. Lamy de la Chapelle, S. Lefrant, P. Deniard, R. Lee, and J. E. Fisher, Nature (London) **388**, 756 (1997).
[5] H. M. Cheng, F. Li, G. Su, H. Y. Pan, L. L. He, X. Sun, and M. S. Dresselhaus, Appl. Phys. Lett. **72**, 3282 (1998).
[6] B. C. Satiskumar, A. Govindaraj, R. Sen, and C. N. R. Rao, Chem. Phys. Lett. **293**, 47 (1998).
[7] M. Yudasaka, T. Ichihashi, T. Komatsu, and S. Iijima, Chem. Phys. Lett. **299**, 91 (1999).
[8] S. Arepalli and C. D. Scott, Chem. Phys. Lett. **302**, 139 (1999).
[9] F. Kokai, K. Takahashi, M. Yudasaka, R. Yamada, T. Ichihashi, and S. Iijima, J. Phys. Chem. **B103**, 4346 (1999).
[10] D. B. Geohegan, A. A. Puretzky, G. Duscher, and S. J. Pennycook, Appl. Phys. Lett. **72**, 2987 (1998).
[11] D. B. Geohagan, A. A. Puretzky, G. Duscher, and S. J. Pennycook, Appl. Phys. Lett. **73**, 438 (1998).
[12] D. B. Geohegan, A. A. Puretzky, and D. J. Rader, Appl. Phys. Lett. **74**, 3788 (1999).
[13] D. B. Geohegan, A. A. Puretzky, R. L. Hettich, X.-Y. Zheng, R. E. Haufler, and R. N. Compton, Trans. Mater. Res. Soc. Jpn. **17**, 349 (1994).
[14] Images also available online at www.ornl.gov/~odg.
[15] A. V. Bulgakov and N. M. Bulgakova, J. Phys. D: Appl. Phys. **31**, 693 (1998).
[16] F. Garrelie, C. Champeaux, and A. Catherinot, Appl. Phys. A: Mater. Sci. Process. **69**, 45 (1999).
[17] D. B. Geohegan and A. A. Puretzky, Mater. Res. Soc. Symp. Proc. **397**, 55 (1996).
[18] E. A. Rohlfing, J. Chem. Phys. **89**, 6103 (1988).
[19] M. Yudasaka, R. Yamada, N. Sensui, T. Wilkins, T. Ichihashi, and S. Iijima, J. Phys. Chem. B **103**, 6224 (1999).